BIOMOLECULES

10.1126/sciadv.1501397

Template-dependent nucleotide addition in the reverse (3′-5′) direction by Thg1-like protein

Shoko Kimura,[1]* Tateki Suzuki,[1]* Meirong Chen,[1] Koji Kato,[1,2] Jian Yu,[2] Akiyoshi Nakamura,[3] Isao Tanaka,[2] Min Yao[1,2†]

Thg1-like protein (TLP) catalyzes the addition of a nucleotide to the 5′-end of truncated transfer RNA (tRNA) species in a Watson-Crick template–dependent manner. The reaction proceeds in two steps: the activation of the 5′-end by adenosine 5′-triphosphate (ATP)/guanosine 5′-triphosphate (GTP), followed by nucleotide addition. Structural analyses of the TLP and its reaction intermediates have revealed the atomic detail of the template-dependent elongation reaction in the 3′-5′ direction. The enzyme creates two substrate binding sites for the first- and second-step reactions in the vicinity of one reaction center consisting of two Mg^{2+} ions, and the two reactions are executed at the same reaction center in a stepwise fashion. When the incoming nucleotide is bound to the second binding site with Watson-Crick hydrogen bonds, the 3′-OH of the incoming nucleotide and the 5′-triphosphate of the tRNA are moved to the reaction center where the first reaction has occurred. That the 3′-5′ elongation enzyme performs this elaborate two-step reaction in one catalytic center suggests that these two reactions have been inseparable throughout the process of protein evolution. Although TLP and Thg1 have similar tetrameric organization, the tRNA binding mode of TLP is different from that of Thg1, a $tRNA^{His}$-specific G_{-1} addition enzyme. Each $tRNA^{His}$ binds to three of the four Thg1 tetramer subunits, whereas in TLP, tRNA only binds to a dimer interface and the elongation reaction is terminated by measuring the accepter stem length through the flexible β-hairpin. Furthermore, mutational analyses show that $tRNA^{His}$ is bound to TLP in a similar manner as Thg1, thus indicating that TLP has a dual binding mode.

INTRODUCTION

All polynucleotide chain elongation reactions, whether with DNA or RNA, proceed in the 5′-3′ direction. This reaction involves the nucleophilic attack of a 3′-OH of the terminal nucleotide in the elongating chain on the α-phosphate of an incoming nucleotide. The energy in the high-energy bond of the incoming nucleotide is used for its addition [termed tail polymerization (*1*)]. This elongation reaction of DNA/RNA chains is in clear contrast to the elongation of protein chains in which the high energy of the incoming aminoacyl-tRNA is not used for its own addition but for the addition of the next monomer (termed head polymerization). However, recent studies have shown that the Thg1/Thg1-like protein (TLP) family of proteins extends tRNA nucleotide chains in the reverse (3′-5′) direction (*2*, *3*). In this case, the 5′-end of tRNA is first activated using adenosine 5′-triphosphate (ATP)/guanosine 5′-triphosphate (GTP), followed by nucleophilic attack of a 3′-OH on the incoming nucleotide [nucleoside 5′-triphosphate (NTP)] to yield pppN-tRNA. Thus, the energy in the triphosphate bond of the incoming nucleotide is not used for its own addition but is reserved for subsequent polymerization (that is, head polymerization) (Fig. 1).

The best-characterized member of this family of proteins is eukaryotic Thg1 ($tRNA^{His}$ guanylyltransferase), which catalyzes the nontemplated addition of a guanylate to the 5′-end of immature $tRNA^{His}$ (*4*). This guanosine at position −1 (G_{-1}) of $tRNA^{His}$ is a critical identity element for recognition by the histidyl-tRNA synthase (*5*–*8*). Therefore, Thg1 is essential to the fidelity of protein synthesis in eukaryotes. However, Thg1 homologs or TLPs are found in organisms in which G_{-1} is genetically encoded, and thus, posttranscriptional modification is not required (*9*, *10*). This finding suggests that TLPs may have potential functions other than $tRNA^{His}$ maturation. TLPs have been shown to catalyze 5′-end nucleotide addition to truncated tRNA species in vitro in a Watson-Crick template–dependent manner (*11*). This function of TLPs is not limited to $tRNA^{His}$ but occurs efficiently with other tRNAs. Furthermore, the yeast homolog (Thg1p) has been shown to interact with the replication origin recognition complex for DNA replication (*12*), and the plant homolog (ICA1) was identified as a protein affecting the capacity to repair DNA damage (*13*). These observations suggest that TLPs may have more general functions in DNA/RNA repair (*3*, *9*, *11*).

The 3′-5′ addition reaction catalyzed by Thg1 occurs through three reaction steps (*4*, *14*). In the first step, the 5′-monophosphorylated $tRNA^{His}$, which is cleaved by ribonuclease P from pre-$tRNA^{His}$, is activated by ATP, creating a 5′-adenylylated $tRNA^{His}$ intermediate. In the second step, the 3′-OH of the incoming GTP attacks the activated intermediate, yielding $pppG_{-1}$-$tRNA^{His}$. Finally, the pyrophosphate is removed, and mature pG_{-1}-$tRNA^{His}$ is created. The crystal structure of human Thg1 (*Hs*Thg1) (*15*) shows that its catalytic core shares structural homology with canonical 5′-3′ nucleotide polymerases, such as T7 DNA/RNA polymerases (*16*, *17*). This finding suggests that 3′-5′ elongation enzymes are related to 5′-3′ polymerases and raises important questions on why 5′-3′ polymerases predominate in nature. The crystal structure of TLP from *Bacillus thuringiensis* shows that it shares a similar tetrameric assembly and active-site architecture with *Hs*Thg1 (*18*). Furthermore, the structure of *Candida albicans* Thg1 (*Ca*Thg1) complexed with $tRNA^{His}$ reveals that the tRNA substrate accesses the reaction center from a direction opposite to that of canonical DNA/RNA polymerase (*19*). However, in this structural analysis, the 5′-end of $tRNA^{His}$ was not activated and the second substrate (GTP) was not bound. Thus, a detailed reaction mechanism remains unknown.

[1]Graduate School of Life Science, Hokkaido University, Sapporo 060-0810, Japan. [2]Faculty of Advanced Life Science, Hokkaido University, Sapporo 060-0810, Japan. [3]Bioproduction Research Institute, National Institute of Advanced Industrial Science and Technology (AIST), Sapporo 062-8517, Japan.
*These authors contributed equally to this work.
†Corresponding author. E-mail: yao@castor.sci.hokudai.ac.jp

Here, we successfully solved the structure of TLP from the methanogenic archaeon *Methanosarcina acetivorans* (*Ma*TLP) in complex with ppptRNA$^{Phe}\Delta_1$, which mimics the activated intermediate of the repair substrate. Although TLP and Thg1 have similar tetrameric organization, the mode of tRNA binding is different in TLP. Furthermore, we obtained the structure in which the GTP analog (GDPNP) was inserted into this complex to form a Watson-Crick base pair with C_{72} at the 3′-end region of the tRNA. On the basis of these structures, we discuss the reaction mechanism of template-dependent reverse (3′-5′) polymerization in comparison with canonical 5′-3′ polymerization.

RESULTS

Anticodon-independent binding of ppptRNA$^{Phe}\Delta_1$ to *Ma*TLP

Previous biochemical experiments have suggested that ppptRNA$^{Phe}\Delta_1$, in which the 5′-end of tRNA^{Phe} was triphosphorylated and G_1 was deleted, can be an efficient substrate for the repair reaction (guanylyl transfer) of Thg1/TLP (*4*, *10*, *20*). Therefore, we prepared a crystal of *Ma*TLP complexed with ppptRNA$^{Phe}\Delta_1$ and solved its structure to study the template-directed 3′-5′ elongation reaction by TLP (fig. S1). The crystal contained a dimer of TLP (A and B molecules) and one tRNA in an asymmetric unit. Two dimers in the crystal further assembled as a dimer of dimers by the crystallographic twofold axis (Fig. 2). This tetrameric structure and 4:2 stoichiometry of the TLP-tRNA complex are the same as those of the *Ca*Thg1-tRNA complex (*19*). However, whereas the AB and CD dimers of tetrameric *Ca*Thg1 play different roles, respectively recognizing the accepter stem and anticodon of tRNA^{His} (*19*), the AB dimer and its symmetry mate (CD dimer) on tetrameric *Ma*TLP independently bind one molecule of tRNA (fig. S2), recognizing the tRNA accepter stem and elbow region. Thus, consistent with the notion that *Ma*TLP is an anticodon-independent repair enzyme (*11*), the anticodon was not recognized in the *Ma*TLP-tRNA complex, whereas the binding mode of *Ca*Thg1 is for the G_{-1} addition reaction, therefore the His anticodon has to be recognized (see "Dual binding mode for tRNA repair").

The elbow region of the tRNA substrate was recognized by the β-hairpin of molecule B of *Ma*TLP. The N atoms in the side chain of R215 in the β-hairpin region of *Ma*TLP were hydrogen-bonded to the phosphate groups of U_{55} and G_{57}. The O atom on the S213 side chain was also hydrogen-bonded to the phosphate moiety of G_{57} of the tRNA (Fig. 2). This β-hairpin region was disordered in the crystal structure of the *Ca*Thg1-tRNA complex.

The accepter stem of the tRNA substrate was recognized by molecule A of *Ma*TLP. The N7 atom of G_2 at the 5′-end was hydrogen-bonded to the N atom of the R136 side chain, whereas the α-phosphate was bonded to the N137 side chain (Fig. 2). R136 was also hydrogen-bonded to the base of C_{72} (the Watson-Crick bond partner of ΔG_1). The triphosphate moiety at the 5′-end of the tRNA was bonded to the D21-K26 region. These phosphates were also coordinated to two metal ions, presumably Mg^{2+} (Mg^{2+}A and Mg^{2+}B) because they were observed at the same positions (figs. S3 and S4) previously identified by *Ca*Thg1 (*19*) and *Hs*Thg1 structures (*15*). These ions were in turn coordinated by the O atoms of the side chains of D21 and D69 and the main-chain O of G22 (fig. S3A). Mutation of D29 and D76 in *Hs*Thg1 (corresponding to D21 and D69 of *Ma*TLP) has been shown to markedly decrease G_{-1} addition activity (*15*).

Template-dependent binding of the GTP analog to the *Ma*TLP-ppptRNA$^{Phe}\Delta_1$ complex

Here, we successfully obtained the structure of the ternary complex of *Ma*TLP, 5′-activated tRNA (ppptRNA$^{Phe}\Delta_1$), and the GTP analog

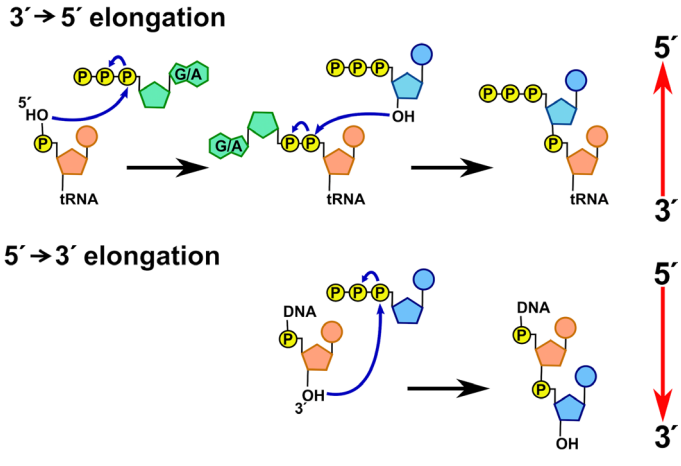

Fig. 1. Reaction schemes of 3′-5′ and 5′-3′ elongation. Top: Reaction scheme of 3′-5′ elongation by Thg1/TLP family proteins. **Bottom:** Reaction scheme of 5′-3′ elongation by DNA/RNA polymerases. In 3′-5′ elongation by Thg1/TLP family proteins, the 5′-monophosphate of the tRNA is first activated by ATP/GTP, followed by the actual elongation reaction. The energy of the incoming nucleotide is not used for its own addition but is reserved for the subsequent addition (head polymerization). In 5′-3′ elongation by DNA/RNA polymerases, the energy of the incoming nucleotide is used for its own addition (tail polymerization).

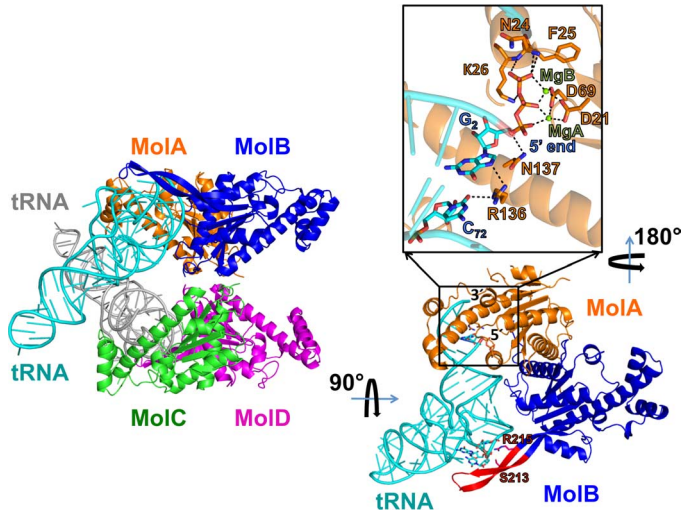

Fig. 2. Structure of the *Ma*TLP complex with ppptRNA$^{Phe}\Delta_1$. Left: One molecule of the tRNA substrate (ppptRNA$^{Phe}\Delta_1$) is bound to the *Ma*TLP dimer. The AB and CD dimers are further dimerized by the crystallographic twofold axis to form a tetrameric structure (dimer of dimers). **Right:** Left figure rotated by 90°. The CD dimer is omitted for clarity. The accepter stem of the tRNA is recognized by molecule A (yellow), and the elbow region by molecule B (blue). Residues important for binding are depicted in stick form. The β-hairpin region of molecule B is shown in red.

(GDPNP) (Fig. 3 and fig. S4) by soaking the *Ma*TLP-ppptRNA$^{Phe}\Delta_1$ complex crystal in a solution containing GDPNP. The obtained structure showed that the guanine base of the incoming GDPNP formed Watson-Crick hydrogen bonds with C_{72} and accompanied base-stacking interactions with G_2 of the tRNA (Fig. 3B), whereas no interaction was observed between the guanine base and the enzyme. These features are consistent with the fact that this elongation reaction is template-dependent. The 5′-end (position 2) of the tRNA moved significantly (Fig. 3C) due to the insertion of GDPNP. Surprisingly, the 5′-triphosphate moiety after movement occupied the GTP/ATP triphosphate position during the activation step (Fig. 3D). Together with the observation that the 3′-OH of the incoming GTP analog was within coordination distance (2.8 Å) to Mg^{2+}A (fig. S3B) and was able to execute a nucleophilic attack on the α-phosphate of the 5′-end, this structure indicates that the elongation reaction (second reaction) takes place at the same reaction center where the activation reaction (first reaction) occurs.

The triphosphate moiety of GDPNP was at the interface between molecules A and B and was recognized by the side chains of both molecules, including R19 (molecule A), R83 (molecule B), K86 (molecule B), and R114 (molecule A) (Fig. 3B). All of these residues are well conserved (fig. S5), and mutation of corresponding residues in *Sc*Thg1 (R27, R93, K96, and R133) decreased the catalytic efficiency of G_{-1} addition (*21*). The triphosphate of the GDPNP was also bonded to the third Mg^{2+} (Mg^{2+}C), which, unlike Mg^{2+}A and Mg^{2+}B, is not coordinated by the TLP molecule (fig. S3B). This triphosphate binding mode is the same as that for the second nucleotide binding site in Thg1. However, in previous analyses, the base moiety at the second site was either invisible (*15*) or far beyond the reaction distance of the phosphate, and therefore, flipping of the base was expected to occur (*19*).

tRNA binding and repair experiments of the β-hairpin mutants

To confirm tRNA recognition by the β-hairpin, we created mutation variants with altered residues in the β-hairpin region. Then, tRNA binding and enzymatic activities were measured. β-Hairpin deletion variant delR198-R215 almost completely abolished the binding of tRNA$^{Phe}\Delta_1$ (fig. S6). Furthermore, the enzymatic activities of delR198-R215 and delG202-E210 were very weak (5.2 and 13.5%, respectively) compared with wild type, whereas mutations (N179A and F174A/N179A/R188A) on the anticodon recognition site [deduced from the Thg1-tRNA^{His} complex structure (*19*)] had no effect on the catalytic activity (Fig. 4A). Experiments using the tRNA$^{His}\Delta_1$ substrate gave similar results (Fig. 4A). All these results are consistent with the crystal structure and suggest that the β-hairpin plays an important role in anticodon-independent binding of the tRNA substrate. Residues in the β-hairpin are not well conserved, except for R215 (fig. S5). Mutants R215A and R215A/S213A, in which the completely conserved R215 was changed to alanine, showed a moderate effect on the activity (27.3 and 16.3%, respectively). Thus, specific interactions with the conserved R215 and van der Waals contacts to residues in the β-hairpin would be important for tRNA recognition.

Termination of the elongation reaction by measuring the accepter stem

TLPs catalyze the Watson-Crick template–dependent elongation or repair reaction for 5′-end truncated tRNA^{Phe} substrates lacking G_1 only (tRNA$^{Phe}\Delta_1$), or lacking both G_1 and G_2 (tRNA$^{Phe}\Delta_{1,2}$) (*11*), whereas they do not show any activity with intact tRNA^{Phe} (thus, repair is unnecessary). How TLP distinguishes between tRNAs that need 5′-end

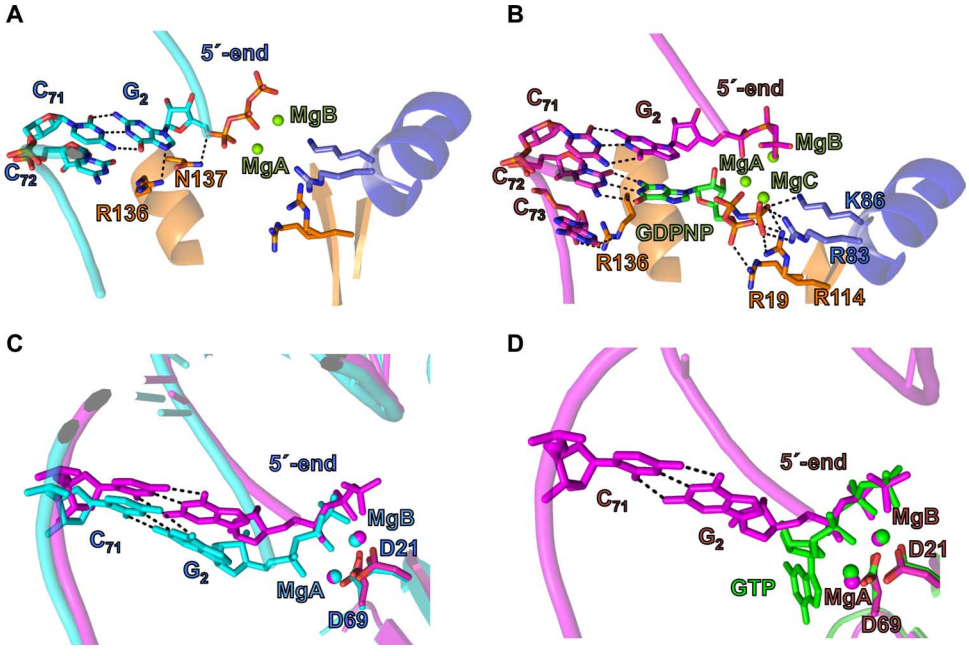

Fig. 3. Structural change of the tRNA (ppptRNA$^{Phe}\Delta_1$). Structural change of the tRNA (ppptRNA$^{Phe}\Delta_1$) accepter stem in *Ma*TLP caused by insertion of GDPNP. (**A**) Structure before GDPNP binding. (**B**) Structure after GDPNP binding. (**C**) Superposition of the two structures showing movement of the 5′-end of the tRNA before (blue) and after (red) insertion of GDPNP. (**D**) Superposition of the 5′-end of the tRNA after GDPNP insertion (red) with GTP at the activation step (green), showing that both triphosphate moieties superpose well.

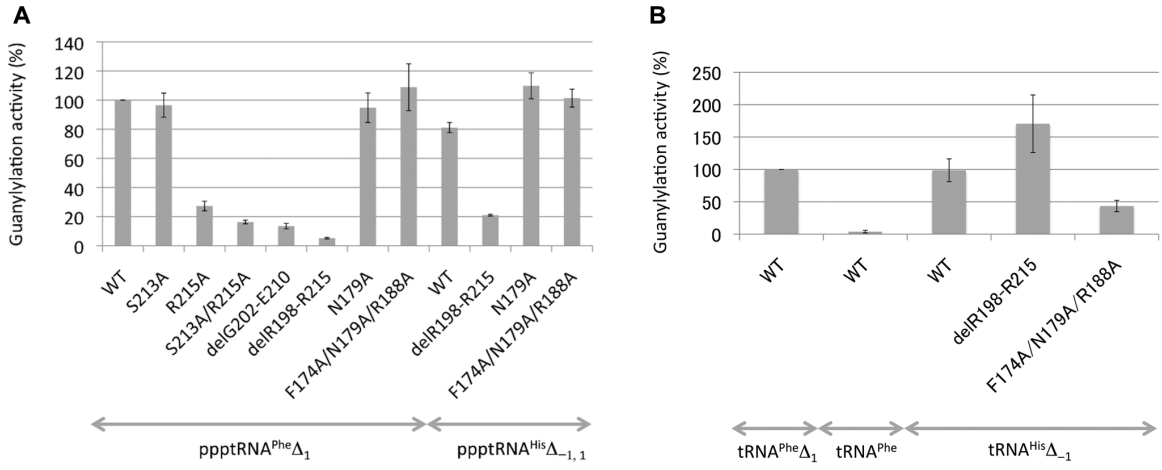

Fig. 4. Mutational analysis of the β-hairpin and anticodon binding region. The rates of guanylylation by various mutants were measured. Error bars represent the SD of three independent experiments. (**A**) Guanylylation of pppRNA$^{Phe}\Delta_1$ and pppRNA$^{His}\Delta_1$ by various TLP mutants. The activity using [α-^{32}P]GTP, wild-type *Ma*TLP, and pppRNA$^{Phe}\Delta_1$ is denoted as 100. (**B**) Guanylylation of tRNA$^{Phe}\Delta_1$, tRNA^{Phe}, and tRNA$^{His}\Delta_{-1}$ by various TLP mutants. The activity to tRNA$^{Phe}\Delta_1$ is about 10% of pppRNA$^{Phe}\Delta_1$.

repair from ones that do not, or in other words, how the elongation reaction is properly terminated, remains unknown. The present structure of the *Ma*TLP-pppRNA$^{Phe}\Delta_1$ complex shows that, unlike Thg1, the TLP dimer binds one molecule of tRNA by recognizing the elbow region by the β-hairpin of molecule B and the 5′-end by molecule A. Therefore, we speculated that the flexible nature of the β-hairpin enables the recognition of tRNA substrates with different accepter stem lengths. To confirm this speculation, we used computer graphics to examine whether the β-hairpin region was able to bind tRNA substrates with different accepter stem lengths when the 5′-end was properly placed in the reaction site. When the 5′-end was placed in the reaction site, the body of the tRNA molecule shifted in a manner dependent on the accepter stem length. The tRNA body also rotated because of the helical nature of the accepter stem (fig. S7). This model structure showed that the accepter stem of intact tRNA^{Phe} was too long for the β-hairpin to recognize its elbow region, whereas tRNA$^{Phe}\Delta_1$ and tRNA$^{Phe}\Delta_{1,2}$ were recognized by the β-hairpin region (fig. S7), which is consistent with previous experiments (*11*). On the basis of these model structures, we concluded that the TLP molecule can properly terminate elongation by measuring the accepter stem length of tRNA substrates.

Dual binding mode for tRNA repair

The present structural analysis revealed that although TLP and Thg1 have a similar tetrameric architecture, they have different binding modes for tRNAs: Thg1 is bound to tRNA^{His} as a tetramer, whereas TLP is bound to tRNA^{Phe} as a dimer. This difference in the tRNA binding modes is closely related to their enzymatic functions. The tRNA^{His}-specific G_{-1} addition enzyme Thg1 needs to recognize both the accepter stem and anticodon of tRNA^{His}. The tetrameric architecture of the Thg1 molecule allows it to access both regions located at the opposite side of the tRNA molecule [the AB dimer recognizes the accepter stem and CD dimer anticodon (*19*)]. In contrast, the binding mode of TLP corresponds to the anticodon-independent repair reactions of 5′-truncated general tRNAs. This binding mode is also suitable for the correct termination of the elongation or repair reaction by measuring the length of the accepter stem by the flexible β-hairpin.

Because tRNA^{His} requires an extra guanosine (G_{-1}) at the 5′-end, the repair enzyme has to extend the 5′-end by one more nucleotide than other tRNAs. TLP has been shown to confer such catalytic activity on tRNA$^{His}\Delta_{-1}$ (Fig. 4B) (*11*). Here, we showed that the TLP mutants, wherein the β-hairpin is truncated and tRNA$^{Phe}\Delta_1$ binding ability is lost, can still bind to tRNA^{Phe} (GUG) whose anticodon is changed to that for His (fig. S6, C, H, and I). Also, the intact tRNA^{Phe}, which is not recognized by TLP (Fig. 4B and fig. S6E), can be recognized when its anticodon is changed to that for His (fig. S6D). Furthermore, the TLP variant (F174A/N179A/R188A) whose anticodon recognition site [deduced from the Thg1-tRNA^{His} complex structure (*19*)] is disrupted has been shown to have a reduced catalytic activity to tRNA$^{His}\Delta_{-1}$ (Fig. 4B). All these experimental results indicate that TLP recognizes and binds tRNAs carrying the His anticodon in the same way that Thg1 recognizes tRNA^{His}. Thus, we concluded that TLP has two tRNA binding modes that are selectively used, depending on both the length of the accepter stem and the anticodon. The elongation or repair reaction normally terminates when the 5′-end reaches position 1, but when the His anticodon is present, TLP binds the tRNA in the second mode by recognizing the anticodon to execute the G_{-1} addition reaction. By having two different binding modes, TLP can manage this special feature of tRNA^{His}.

DISCUSSION

The Thg1/TLP family of proteins extends tRNA chains in the 3′-5′ direction. The reaction involves two steps. First, the 5′-phosphate is activated by GTP/ATP. Then, the activated phosphate is attacked by the incoming nucleotide, resulting in an extension by one nucleotide at the 5′-end (*4*, *14*). Here, we successfully solved for the first time the intermediate structures of the template-dependent 3′-5′ elongation complex of *Ma*TLP. On the basis of these structures, we will discuss

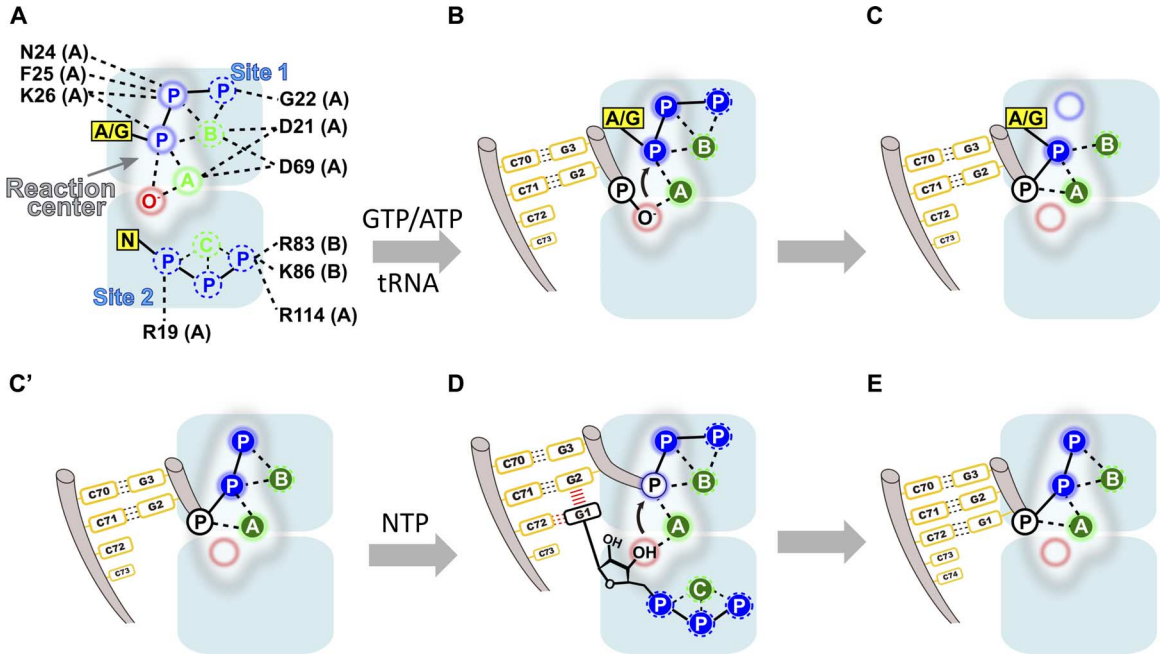

Fig. 5. Schematic representation of the 3′-5′ elongation mechanism. (**A**) The reaction center overlapped with two triphosphate binding sites. A, B, and C (in green) represent binding sites for Mg^{2+}A, Mg^{2+}B, and Mg^{2+}C. P (in blue) represents the phosphate binding sites; O^- (in red) is the binding site for the deprotonated OH group. Important TLP residues for tRNA and Mg^{2+} binding are also shown. (**B**) Structure of the activation complex (corresponding to fig. S8). GTP/ATP binds to triphosphate binding site 1; the deprotonated OH group of the 5′-phosphate attacks the α-phosphate of GTP/ATP, and PPi (inorganic pyrophosphate) is released. (**C**) Possible structure after the activation step as suggested from the structure of (C′). (**C′**) Structure before the elongation reaction (corresponding to Fig. 3A). The 5′-triphosphate of the tRNA binds to the same site as for activation of the 5′-terminus of the tRNA in (B). (**D**) Structure of initiation of the elongation reaction (corresponding to Fig. 3B). The base of the incoming GTP forms a Watson-Crick hydrogen bond with the nucleotide at position 72 in the template chain and a base-stacking interaction with a neighboring base (G2). Movement of the 5′-terminal chain leaves the 5′-triphosphate of the tRNA in the same site as the activation step in (B). The 3′-OH of the incoming GTP is deprotonated by Mg^{2+}A and attacks the α-phosphate to form a covalent bond. (**E**) After the elongation reaction, the triphosphate of the new nucleotide is placed on site 1, as in (C′), and is ready for the next reaction.

the 3′-5′ addition reaction compared with canonical 5′-3′ elongation by DNA/RNA polymerases.

Figure 5 is a schematic diagram of the 3′-5′ addition reaction of TLP. This enzyme has two triphosphate binding sites and one reaction center at the position overlapping these two binding sites (Fig. 5A). In the first activation step, when GTP/ATP is bound to site 1 (Fig. 5B), the 5′-phosphate of the tRNA is deprotonated by Mg^{2+}A and attacks the α-phosphate of the GTP/ATP, resulting in an activated intermediate (Fig. 5C). The structure of the *Ma*TLP-ppptRNA$^{Phe}\Delta_1$ complex, wherein β- and γ-phosphates coordinate with Mg^{2+}A and Mg^{2+}B, respectively (Figs. 3A and 5C′), may represent this activated intermediate. Subsequent binding of an incoming nucleotide to site 2 followed by formation of the Watson-Crick base pair with a nucleotide in the template strand conveys the 3′-OH of the incoming nucleotide to the position of deprotonation by Mg^{2+}A and the 5′-triphosphate of the tRNA to the reaction center (Figs. 3B and 5D). Then, the elongation reaction of step 2 occurs (Fig. 5E). Thus, the present structure shows that this 3′-5′ elongation enzyme utilizes a reaction center homologous to that of 5′-3′ elongation enzymes for both activation and elongation in a stepwise fashion. Although these two reactions are similar in chemistry, their substrate characteristics are very different. It should be noted that TLP has evolved to allow the occurrence of these two elaborate reaction steps within one reaction center.

Figure 6 compares the 3′-5′ and 5′-3′ elongation mechanisms, showing the symmetrical nature of both elongation reactions using a similar reaction center composed of Mg^{2+}A and Mg^{2+}B in the conserved catalytic core. In TLP, which carries out 3′-5′ elongation, the 3′-OH of the incoming nucleotide attacks the 5′-activated phosphate of the tRNA to form a phosphodiester bond, whereas in the T7 RNA polymerase, a representative 5′-3′ DNA/RNA polymerase, the 3′-OH of the 3′-terminal nucleotide of the RNA attacks the activated phosphate of the incoming nucleotide to form a phosphodiester bond. In these reactions, the roles of the two Mg ions are identical. Mg^{2+}A activates the 3′-OH of the incoming nucleotide in TLP and the 3′-OH of the 3′-end of the RNA chain in T7 RNA polymerase. The role of Mg^{2+}B is to position the 5′-triphosphate of the tRNA in TLP and the incoming nucleotide in T7 RNA polymerase. These two Mg^{2+} ions are coordinated by a conserved Asp (D21 and D69 in TLP) in the conserved catalytic core.

Because the chemical roles of tRNA and the incoming nucleotide are reversed in these two reactions, these two substrates are inserted into a similar reaction center from opposite directions (Fig. 6). In spite of this difference, their fundamental reaction scheme is conserved. However, from an energetic viewpoint, these two reactions are clearly different: Whereas the high energy of the incoming nucleotide is used for its own addition in DNA/RNA polymerases, the high energy of the

incoming nucleotide is used for subsequent addition in TLP. For this reason, TLP requires a mechanism that activates the 5′-terminus of the tRNA during the initial step of the reaction. Our analysis showed that the initial activation and subsequent elongation reactions occur sequentially at one reaction center. In this case, the enzyme needs to create two substrate binding sites for two different reactions in the vicinities of one reaction center. TLP has successfully created such sites by utilizing a conformational change in the tRNA through Watson-Crick base pairing (Fig. 3). These structural features of the TLP molecule suggest that development of an activation reaction site is a prerequisite for developing the 3′-5′ elongation enzyme. This is clearly more difficult than developing the 5′-3′ elongation enzyme, wherein the activation reaction site is not necessary, and which may be the primary reason why the 5′-3′ elongation enzyme has been exclusively developed.

Here, we established a structural basis for 3′-5′ nucleotide elongation and showed that TLP has evolved to acquire a two-step Watson-Crick template–dependent 3′-5′ elongation reaction using the catalytic center homologous to 5′-3′ elongation enzymes. The active site of this enzyme is created at the dimerization interface. The dimerization also endows this protein with the ability to measure the length of the accepter stem of the tRNA substrate, so that the enzyme can properly terminate the elongation reaction. Furthermore, the dual binding mode of this protein suggests that it has further evolved to cover G_{-1} addition of $tRNA^{His}$ by additional dimerization (dimer of dimers). Thus, the present structural analysis is consistent with the scenario in which TLP began as a 5′-end repair enzyme and evolved into a $tRNA^{His}$-specific G_{-1} addition enzyme. The detailed molecular mechanism of the Thg1/TLP family established by our analysis will open up new perspectives in our understanding of 3′-5′ versus 5′-3′ polymerization and the molecular evolution of template-dependent polymerases.

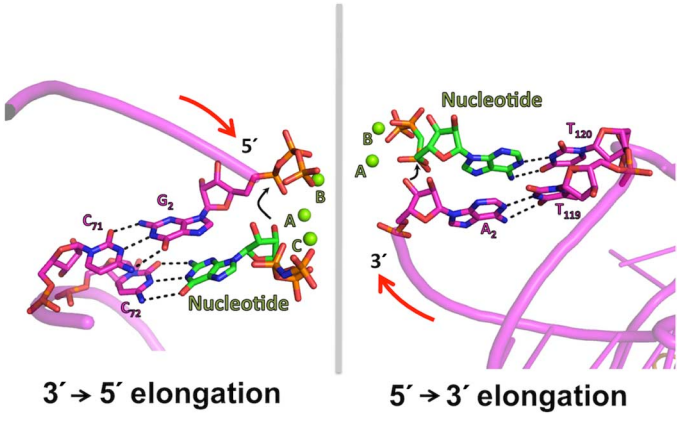

Fig. 6. Structures of template-dependent nucleotide elongation in the 3′-5′ and 5′-3′ directions. Symmetrical relationship between 3′-5′ elongation by TLP (this study) (left) and 5′-3′ elongation by T7 RNA polymerase [Protein Data Bank (PDB) ID: 1S76] (right). Red arrows represent elongation directions. In the 3′-5′ elongation reaction, the 3′-OH of the incoming nucleotide attacks the 5′-activated phosphate of the tRNA to form a phosphodiester bond, whereas in the 5′-3′ elongation reaction, the 3′-OH of the 3′-terminal nucleotide of the RNA attacks the activated phosphate of the incoming nucleotide to form a phosphodiester bond. Green spheres represent Mg^{2+} ions.

MATERIALS AND METHODS

Plasmid construction

Genomic DNA from *M. acetivorans* NBRC100939 was obtained from the NITE Biological Resource Center. The *Ma*TLP gene was amplified by polymerase chain reaction from genomic DNA. The DNA fragment encoding *Ma*TLP was then cloned between the Nde I and Xho I restriction sites in a pET26b vector with a C-terminal His tag. In the *Ma*TLP gene, the amber stop codon (UAG) at position 142 was translated as Pyl. To express the full-length *Ma*TLP in *Escherichia coli*, the TAG codon was altered to TGG (encoding Trp) with the QuikChange Site-Directed Mutagenesis Kit (Agilent Technologies) as previously described (*9*, *22*). The inserted sequence was verified by DNA sequencing.

Preparation of *Ma*TLP and mutants

Plasmids were transformed into *E. coli* strain BL21 (DE3) pLysSRARE by electroporation, and cells were grown in LB medium containing kanamycin (25 μg/ml) and chloramphenicol (34 μg/ml) at 37°C until reaching an optical density at 600 nm (OD_{600}) of 0.45. The cells were then induced by the addition of isopropyl-β-D-thiogalactopyranoside to a final concentration of 250 μM and shifted to 18°C for approximately 20 hours before harvest. The cells were harvested and resuspended in buffer A [50 mM Hepes-NaOH (pH 7.5), 1 M NaCl, 4 mM $MgCl_2$, 10% glycerol, 0.5 mM β-mercaptoethanol, lysozyme (0.5 mg/ml), and deoxyibonuclease (0.1 mg/ml)]. After sonication and centrifugation, the His_6-tagged protein was purified by immobilized metal-ion affinity chromatography using a HisTrap HP column (GE Healthcare). The sample was washed with 75 mM imidazole and eluted with a 75 to 400 mM imidazole gradient in buffer B [50 mM tris-HCl (pH 7.5), 500 mM NaCl, 4 mM $MgCl_2$, 20% glycerol, and 0.5 mM β-mercaptoethanol]. Then, the collected fractions were diluted in 300 mM NaCl with buffer C [25 mM tris-HCl (pH 7.5), 10% glycerol, 5 mM $MgCl_2$, and 1 mM dithiothreitol (DTT)] and further purified on a HiTrap Heparin HP column (GE Healthcare) by elution with a 300 to 1000 mM NaCl gradient in buffer C. Finally, the protein was loaded onto a HiLoad 16/60 Superdex 200 prep grade column (GE Healthcare) equilibrated with buffer D [20 mM Hepes-NaOH (pH 7.5), 500 mM NaCl, 5 mM $MgCl_2$, 10% glycerol, and 1 mM DTT]. The protein was concentrated to 3.9 mg/ml by ultrafiltration. All *Ma*TLP mutants were constructed with the QuikChange Site-Directed Mutagenesis Kit. *Ma*TLP mutants were purified by a HisTrap HP column for RNA binding assay and further purified by a HiLoad 16/60 Superdex 200 prep grade column for 3′-5′ nucleotide addition assay.

Preparation of tRNA and its mutants

tRNA transcripts derived from yeast $tRNA^{Phe}$ and $tRNA^{His}$ were prepared using T7 RNA polymerase as previously described (*19*). pppt RNA transcripts were prepared by excluding guanosine 5′-monophosphate (GMP) from the reaction mixture. Transcribed tRNAs were purified by a HiTrap DEAE FF column (GE Healthcare) as previously described (*23*). Pooled tRNAs were precipitated with isopropanol and dissolved in buffer E [20 mM Hepes-NaOH (pH 7.5), 100 mM NaCl, and 10 mM $MgCl_2$].

Preparation of the *Ma*TLP-ppptRNA$^{Phe}\Delta_1$ complex

*Ma*TLP and ppptRNA$^{Phe}\Delta_1$ ($tRNA^{Phe}$ with a triphosphorylated 5′-end and deleted G_1) were mixed in a molar ratio of 1.7:1 and incubated for 30 min at room temperature. The mixture was then loaded

onto a HiLoad 16/60 Superdex 200 prep grade column equilibrated with buffer F [20 mM Hepes-NaOH (pH 7.5), 400 mM NaCl, 5 mM $MgCl_2$, 10% glycerol, and 1 mM DTT]. Fractions containing the *Ma*TLP-ppptRNA$^{Phe}\Delta_1$ complex were mixed with 1 mM spermine and concentrated to an OD_{280} of 16 by ultrafiltration.

Crystallization and data collection

All crystallization experiments were performed with the sitting-drop vapor diffusion method at 293 K. Initial crystals of *Ma*TLP were obtained by mixing 1 μl of protein solution (3.9 mg/ml) with 1 μl of a reservoir solution containing 0.1 M Hepes-NaOH buffer (pH 7.5), 0.2 M magnesium chloride, and 30% polyethylene glycol 400 (PEG 400). *Ma*TLP-GTP complex crystals were obtained by soaking the *Ma*TLP crystals in the above reservoir solution supplemented with 1 mM GTP overnight. High-resolution crystals of *Ma*TLP in apo form (*Ma*TLP-apo) were obtained unexpectedly by mixing *Ma*TLP with tRNA^{His} in 0.1 M sodium/potassium phosphate (pH 6.2) containing 2.5 M NaCl. Crystals of the *Ma*TLP-ppptRNA$^{Phe}\Delta_1$ complex were obtained from a solution containing 0.2 M tripotassium citrate, 0.1 M tris (pH 8.0), 37% PEG3350, and 10 mM praseodymium (III) acetate. Crystals of the *Ma*TLP-ppptRNA$^{Phe}\Delta_1$-GDPNP complex were obtained by soaking *Ma*TLP-ppptRNA$^{Phe}\Delta_1$ complex crystals in a reservoir solution containing 0.2 M tripotassium citrate, 0.1 M tris (pH 8.0), 30% PEG3350, 5% glycerol, and 15 mM GDPNP overnight. Crystals of

Table 1. Summary of data collection and refinement statistics. Values in parentheses are for the highest-resolution shell. PF, Photon Factory; Rmsd, root-mean-square deviation.

	*Ma*TLP-apo	*Ma*TLP-GTP	*Ma*TLP-ppptRNA$^{Phe}\Delta_1$	*Ma*TLP-ppptRNA$^{Phe}\Delta_1$-GDPNP
PDB ID	5AXK	5AXL	5AXM	5AXN
Data collection				
Beamline	SPring-8 BL41XU	SPring-8 BL41XU	PF BL17A	PF BL5A
Space group	$C222_1$	$C222_1$	*I*222	*I*222
Unit cell parameters *a*, *b*, *c* (Å)	98.3, 120.5, 157.4	103.1, 115.7, 144.9	75.3, 127.6, 143.8	82.3, 134.1, 147.4
Wavelength (Å)	0.9780	1.0000	0.97319	1.0000
Resolution range (Å)	50.0–2.29 (2.43–2.29)	50.0–2.99 (3.17–2.99)	50.0–2.21 (2.34–2.21)	50.0–2.70 (2.87–2.70)
R_{meas} (%)*	8.9 (76.3)	15.2 (90.0)	9.7 (74.4)	11.0 (87.2)
$CC_{1/2}$ (%)	99.8 (80.4)	99.5 (81.2)	99.9 (83.6)	99.9 (83.5)
$\langle I/\sigma(I)\rangle$	14.7 (2.8)	12.0 (2.6)	19.4 (3.2)	16.9 (2.5)
Completeness (%)	98.3 (93.8)	98.8 (93.4)	99.7 (98.6)	99.7 (99.3)
Redundancy	6.7 (6.6)	7.2 (7.2)	7.4 (7.3)	8.1 (8.2)
Refinement				
No. of reflections	41,650	17,581	35,102	22,669
R_{work}/R_{free} (%)†	20.6/24.0	21.5/25.3	21.6/24.3	22.5/26.7
No. of atoms				
Macromolecules	3760	3622	5247	5142
Ligand/ion	30	68	36	101
Water	89	8	102	16
B-factors (Å^2)				
Macromolecules	57.0	68.4	45.3	57.3
Ligand/ion	60.5	86.2	46.6	59.9
Water	49.0	59.5	33.0	38.1
Estimated coordinate error (Å)	0.32	0.48	0.25	0.41
Rmsd from ideal				
Bond lengths (Å)	0.009	0.003	0.003	0.003
Bond angles (°)	1.11	0.92	0.72	0.80

*$R_{meas} = \Sigma_{hkl} \{N(hkl)/[N(hkl) - 1]\}^{1/2} \Sigma_i | I_i(hkl) - \langle I(hkl)\rangle | / \Sigma_{hkl} \Sigma_i I_i(hkl)$, where $\langle I(hkl)\rangle$ and $N(hkl)$ are the mean intensity of a set of equivalent reflections and the multiplicity, respectively.
†$R_{work} = \Sigma_{hkl} ||F_{obs}| - |F_{calc}|| / \Sigma_{hkl} |F_{obs}|$; R_{free} was calculated for 5% randomly selected test sets that were not used in the refinement.

*Ma*TLP-apo and *Ma*TLP-GTP were cryoprotected with a reservoir solution containing 50% PEG400 before flash-cooling, whereas crystals of the *Ma*TLP-pppt$RNA^{Phe}\Delta_1$-GDPNP and *Ma*TLP-pppt$RNA^{Phe}\Delta_1$ complexes were flash-cooled without any cryoprotectant under a stream of liquid nitrogen at 100 K. X-ray diffraction data were collected from beamline BL41XU at SPring-8 (Hyogo, Japan) and beamlines BL5A and BL17A at Photon Factory (Ibaraki, Japan). All diffraction data were indexed, integrated, scaled, and merged using XDS (*24*).

Structure determination and refinement

The crystal structure of *Ma*TLP-apo was determined by the molecular replacement (MR) method with Molrep (*25*, *26*), using the protomer structure of *Ca*Thg1 (PDB ID: 3WBZ) (*19*) as a search model. The protomer structure of *Ma*TLP-apo was then used as a search model to solve the structures of *Ma*TLP-GTP. The crystal structure of the *Ma*TLP-pppt$RNA^{Phe}\Delta_1$ complex was determined by the MR method with PHASER (*27*), using the protomer structures of *Ma*TLP-apo and $tRNA^{Phe}$ from *Saccharomyces cerevisiae* (PDB ID: 1EHZ) (*28*) as search models. The structure of the *Ma*TLP-pppt$RNA^{Phe}\Delta_1$ complex was then used as a search model to solve the *Ma*TLP-pppt$RNA^{Phe}\Delta_1$-GDPNP complex structure. Initial protein models were fitted manually using Coot (*29*), and tRNA models were automatically rebuilt by LAFIRE_NAFIT (*30*); these models were then refined using phenix.refine (*31*). The data collection and refinement statistics are summarized in Table 1. All structure figures were generated by PyMol (*32*).

Nucleotide addition assay

Nucleotide addition assays were performed as previously described (*4*). A reaction mixture containing 25 mM Hepes-NaOH (pH 7.5), 400 mM NaCl, 10 mM $MgCl_2$, 3 mM DTT, 5% glycerol, 0.1 μM [α-^{32}P]GTP, 100 μM GTP, 1 μM *Ma*TLP variants, and 10 μM tRNA transcript was incubated at 30°C for 2 hours. Then, the reaction was quenched with phenol/chloroform, and the supernatant was resolved on a 10% polyacrylamide gel containing 8 M urea. The radioactivity was visualized with a BAS-1800 II bioimaging analyzer (Fujifilm).

tRNA binding assay

A reaction mixture containing 34 μM *Ma*TLP variants and 20 μM tRNA transcript was incubated in buffer F at room temperature for 30 min. Then, the mixture was loaded onto a Superdex 200 10/300 GL column (GE Healthcare) equilibrated with the same buffer.

SUPPLEMENTARY MATERIALS

Supplementary material for this article is available at http://advances.sciencemag.org/cgi/content/full/2/3/e1501397/DC1

Fig. S1. Structure of *Ma*TLP-pppt$RNA^{Phe}\Delta_1$ with the final $2F_o - F_c$ map.
Fig. S2. Comparison of the tRNA binding structures of *Ma*TLP and *Ca*Thg1.
Fig. S3. Stereo drawings of the *Ma*TLP active center.
Fig. S4. Structure of the active center in the *Ma*TLP-pppt$RNA^{Phe}\Delta_1$-GDPNP complex superposed with an omit map.
Fig. S5. Multiple sequence alignment of Thg1/TLP enzymes.
Fig. S6. tRNA binding experiments using gel filtration.
Fig. S7. Binding models of TLP and tRNA truncation variants.
Fig. S8. A model of the active center in the activation complex.

REFERENCES AND NOTES

1. B. Alberts, A. Johnson, J. Lewis, M. Raff, K. Roberts, P. Walter, *Molecular Biology of the Cell* (Garland Science, New York, ed. 5, 2008).
2. I. U. Heinemann, A. Nakamura, P. O'Donoghue, D. Eiler, D. Söll, $tRNA^{His}$-guanylyltransferase establishes $tRNA^{His}$ identity. *Nucleic Acids Res.* **40**, 333–344 (2012).
3. J. E. Jackman, J. M. Gott, M. W. Gray, Doing it in reverse: 3′-to-5′ polymerization by the Thg1 superfamily. *RNA* **18**, 886–899 (2012).
4. W. Gu, J. E. Jackman, A. J. Lohan, M. W. Gray, E. M. Phizicky, $tRNA^{His}$ maturation: An essential yeast protein catalyzes addition of a guanine nucleotide to the 5′ end of $tRNA^{His}$. *Genes Dev.* **17**, 2889–2901 (2003).
5. L. Cooley, B. Appel, D. Söll, Post-transcriptional nucleotide addition is responsible for the formation of the 5′ terminus of histidine tRNA. *Proc. Natl. Acad. Sci. U.S.A.* **79**, 6475–6479 (1982).
6. H. Himeno, T. Hasegawa, T. Ueda, K. Watanabe, K.-i. Miura, M. Shimizu, Role of the extra G-C pair at the end of the acceptor stem of $tRNA^{Hb}$ in aminoacylation. *Nucleic Acids Res.* **17**, 7855–7863 (1989).
7. J. Rudinger, C. Florentz, R. Giegé, Histidylation by yeast HisRS of tRNA or tRNA-like structure relies on residues −1 and 73 but is dependent on the RNA context. *Nucleic Acids Res.* **22**, 5031–5037 (1994).
8. A. E. Rosen, K. Musier-Forsyth, Recognition of G-1:C73 atomic groups by *Escherichia coli* histidyl-tRNA synthetase. *J. Am. Chem. Soc.* **126**, 64–65 (2004).
9. M. G. Abad, B. S. Rao, J. E. Jackman, Template-dependent 3′–5′ nucleotide addition is a shared feature of $tRNA^{His}$ guanylyltransferase enzymes from multiple domains of life. *Proc. Natl. Acad. Sci. U.S.A.* **107**, 674–679 (2010).
10. I. U. Heinemann, L. Randau, R. J. Tomko Jr., D. Söll, 3′–5′ $tRNA^{His}$ guanylyltransferase in bacteria. *FEBS Lett.* **584**, 3567–3572 (2010).
11. B. S. Rao, E. L. Maris, J. E. Jackman, tRNA 5′-end repair activities of $tRNA^{His}$ guanylyltransferase (Thg1)-like proteins from Bacteria and Archaea. *Nucleic Acids Res.* **39**, 1833–1842 (2011).
12. T. S. Rice, M. Ding, D. S. Pederson, N. H. Heintz, The highly conserved $tRNA^{His}$ guanylyltransferase Thg1p interacts with the origin recognition complex and is required for the G_2/M phase transition in the yeast *Saccharomyces cerevisiae*. *Eukaryot. Cell* **4**, 832–835 (2005).
13. W. Zhu, I. Ausin, A. Seleznev, B. Méndez-Vigo, F. X. Picó, S. Sureshkumar, V. Sundaramoorthi, D. Bulach, D. Powell, T. Seemann, C. Alonso-Blanco, S. Balasubramanian, Natural variation identifies *ICARUS1*, a universal gene required for cell proliferation and growth at high temperatures in *Arabidopsis thaliana*. *PLOS Genet.* **11**, e1005085 (2015).
14. D. Jahn, S. Pande, Histidine tRNA guanylyltransferase from *Saccharomyces cerevisiae*. II. Catalytic mechanism. *J. Biol. Chem.* **266**, 22832–22836 (1991).
15. S. J. Hyde, B. E. Eckenroth, B. A. Smith, W. A. Eberley, N. H. Heintz, J. E. Jackman, S. Doublié, $tRNA^{His}$ guanylyltransferase (THG1), a unique 3′-5′ nucleotidyl transferase, shares unexpected structural homology with canonical 5′-3′ DNA polymerases. *Proc. Natl. Acad. Sci. U.S.A.* **107**, 20305–20310 (2010).
16. S. Doublié, S. Tabor, A. M. Long, C. C. Richardson, T. Ellenberger, Crystal structure of a bacteriophage T7 DNA replication complex at 2.2 Å resolution. *Nature* **391**, 251–258 (1998).
17. D. Jeruzalmi, T. A. Steitz, Structure of T7 RNA polymerase complexed to the transcriptional inhibitor T7 lysozyme. *EMBO J.* **17**, 4101–4113 (1998).
18. S. J. Hyde, B. S. Rao, B. E. Eckenroth, J. E. Jackman, S. Doublié, Structural studies of a bacterial $tRNA^{His}$ guanylyltransferase (Thg1)-like protein, with nucleotide in the activation and nucleotidyl transfer sites. *PLOS One* **8**, e67465 (2013).
19. A. Nakamura, T. Nemoto, I. U. Heinemann, K. Yamashita, T. Sonoda, K. Komoda, I. Tanaka, D. Söll, M. Yao, Structural basis of reverse nucleotide polymerization. *Proc. Natl. Acad. Sci. U.S.A.* **110**, 20970–20975 (2013).
20. J. E. Jackman, E. M. Phizicky, $tRNA^{His}$ guanylyltransferase adds G_{-1} to the 5′ end of $tRNA^{His}$ by recognition of the anticodon, one of several features unexpectedly shared with tRNA synthetases. *RNA* **12**, 1007–1014 (2006).
21. J. E. Jackman, E. M. Phizicky, Identification of critical residues for G_{-1} addition and substrate recognition by $tRNA^{His}$ guanylyltransferase. *Biochemistry* **47**, 4817–4825 (2008).
22. I. U. Heinemann, P. O'Donoghue, C. Madinger, J. Benner, L. Randau, C. J. Noren, D. Söll, The appearance of pyrrolysine in $tRNA^{His}$ guanylyltransferase by neutral evolution. *Proc. Natl. Acad. Sci. U.S.A.* **106**, 21103–21108 (2009).
23. L. E. Easton, Y. Shibata, P. J. Lukavsky, Rapid, nondenaturing RNA purification using weak anion-exchange fast performance liquid chromatography. *RNA* **16**, 647–653 (2010).
24. W. Kabsch, XDS. *Acta Crystallogr. D Biol. Crystallogr.* **66**, 125–132 (2010).
25. A. Vagin, A. Teplyakov, Molecular replacement with *MOLREP*. *Acta Crystallogr. D Biol. Crystallogr.* **66**, 22–25 (2010).
26. M. D. Winn, C. C. Ballard, K. D. Cowtan, E. J. Dodson, P. Emsley, P. R. Evans, R. M. Keegan, E. B. Krissinel, A. G. W. Leslie, A. McCoy, S. J. McNicholas, G. N. Murshudov, N. S. Pannu, E. A. Potterton, H. R. Powell, R. J. Read, A. Vagin, K. S. Wilson, Overview of the *CCP*4 suite and current developments. *Acta Crystallogr. D Biol. Crystallogr.* **67**, 235–242 (2011).
27. A. J. McCoy, R. W. Grosse-Kunstleve, P. D. Adams, M. D. Winn, L. C. Storoni, R. J. Read, *Phaser* crystallographic software. *J. Appl. Crystallogr.* **40**, 658–674 (2007).
28. H. Shi, P. B. Moore, The crystal structure of yeast phenylalanine tRNA at 1.93 Å resolution: A classic structure revisited. *RNA* **6**, 1091–1105 (2000).

29. P. Emsley, K. Cowtan, *Coot*: Model-building tools for molecular graphics. *Acta Crystallogr. D Biol. Crystallogr.* **60**, 2126–2132 (2004).
30. K. Yamashita, Y. Zhou, I. Tanaka, M. Yao, New model-fitting and model-completion programs for automated iterative nucleic acid refinement. *Acta Crystallogr. D Biol. Crystallogr.* **69**, 1171–1179 (2013).
31. P. D. Adams, P. V. Afonine, G. Bunkóczi, V. B. Chen, I. W. Davis, N. Echols, J. J. Headd, L.-W. Hung, G. J. Kapral, R. W. Grosse-Kunstleve, A. J. McCoy, N. W. Moriarty, R. Oeffner, R. J. Read, D. C. Richardson, J. S. Richardson, T. C. Terwilliger, P. H. Zwart, *PHENIX*: A comprehensive Python-based system for macromolecular structure solution. *Acta Crystallogr. D Biol. Crystallogr.* **66**, 213–221 (2010).
32. W. L. DeLano, *The PyMOL Molecular Graphics System, Version 1.7.4* (Schrödinger, LLC, 2002).

Acknowledgments: The synchrotron radiation experiments were performed with the approval of the Japan Synchrotron Radiation Research Institute (JASRI) (Proposal Nos. 2014B1033 and 2011B1227). We thank the beamline staff of SPring-8 and Photon Factory for their assistance with data collection. **Funding:** This work was supported by Grant-in-Aid for Scientific Research (B) (24370042, to I.T.) from the Ministry of Education, Culture, Sports, Science, and Technology of Japan.
Author contributions: S.K., T.S., and M.C. performed structure biology and biochemical experiments. J.Y., K.K., and M.Y. contributed to the crystallographic calculation. M.Y., T.S., A.N., and I.T. designed the study and planned the experiments. I.T., M.Y., and T.S. wrote the paper. All authors discussed the results and commented on the manuscript. **Competing interests:** The author declare that they have no competing interests. **Data and materials availability:** All data needed to evaluate the conclusions in the paper are present in the paper and/or the Supplementary Materials. Additional data related to this paper may be requested from the authors and the structure factors and atomic coordinates of this study have been deposited in PDB under accession codes 5AXK (*Ma*TLP-apo), 5AXL (*Ma*TLP-GTP), 5AXM (*Ma*TLP-pppt$RNA^{Phe}\Delta_1$), and 5AXN (*Ma*TLP-pppt$RNA^{Phe}\Delta_1$-GDPNP).

Submitted 7 October 2015
Accepted 4 February 2016
Published 25 March 2016
10.1126/sciadv.1501397

Citation: S. Kimura, T. Suzuki, M. Chen, K. Kato, J. Yu, A. Nakamura, I. Tanaka, M. Yao, Template-dependent nucleotide addition in the reverse (3′-5′) direction by Thg1-like protein. *Sci. Adv.* **2**, e1501397 (2016).

Science Advances

Template-dependent nucleotide addition in the reverse (3′-5′) direction by Thg1-like protein

Shoko Kimura, Tateki Suzuki, Meirong Chen, Koji Kato, Jian Yu, Akiyoshi Nakamura, Isao Tanaka and Min Yao

Sci Adv **2** (3), e1501397.
DOI: 10.1126/sciadv.1501397